

Band-edge levels in semiconductors and insulators: Hybrid density functional theory versus many-body perturbation theory

Wei Chen and Alfredo Pasquarello

Chaire de Simulation à l'Echelle Atomique (CSEA), Ecole Polytechnique Fédérale de Lausanne (EPFL), CH-1015 Lausanne, Switzerland

(Received 16 April 2012; revised manuscript received 23 May 2012; published 23 July 2012)

We compare band-edge levels as obtained with hybrid functionals and GW perturbation theory for a wide class of materials. For sp -bonded semiconductors, a close agreement is demonstrated. However, deviations for other materials are more significant and range up to 1 eV for the most ionic insulators. These differences stem from the degree of compensation between exchange and correlation contributions which varies among the band-edge states in GW calculations. Consequently, the two schemes might deliver significantly different level alignments in defect and band-offset studies, particularly when involving wide band-gap materials.

DOI: [10.1103/PhysRevB.86.035134](https://doi.org/10.1103/PhysRevB.86.035134)

PACS number(s): 71.10.-w, 71.15.Mb, 71.55.-i

I. INTRODUCTION

During the last decades, density functional theory (DFT) has evolved into an indispensable tool for the determination of electronic structures. However, the “band-gap problem” associated with the widely adopted (semi)local approximations to the exchange-correlation energy still represents a severe limitation. This drawback is particularly prominent in the determination of the band alignment at semiconductor and oxide interfaces, where band offsets may be underestimated by several electron volts.¹ It also leads to severe ambiguities in the positioning of defect levels within the band gap of semiconductors and insulators.^{2,3}

Many-body perturbation theory in the GW approximation is particularly effective in predicting band structures, and has thus grown into a reference electronic-structure method.^{4,5} The electron self-energy Σ is given by the product of the Green's function G and of the screened Coulomb interaction W .⁶ The fundamental band gap is then obtained from the quasiparticle energies that are solutions of the Dyson equation. The GW approximation has also successfully been applied to band-offset⁷⁻⁹ and defect¹⁰⁻¹⁴ calculations. However, its widespread application is still hampered by the high computational cost involved.

Among the advanced electronic-structure schemes going beyond the semilocal description, hybrid density functionals stand out as an accurate, yet computationally more affordable method. Their applications to a number of defect^{2,15-17} and band-offset calculations^{1,18} show great promise. In these calculations, a fraction of nonlocal Fock exchange is admixed to semilocal exchange in order to increase the band gap. The band-gap opening results from the reduced self-interaction error and from the improved dependence of the total energy on integer number of electrons.¹⁹

It has recently been pointed out that, beyond the band-gap problem, defect and band-offset calculations ultimately depend on the positions of the *band-edge levels*.^{3,20,21} Indeed, the charge transition levels of deep defects are well defined when referenced to the average electrostatic potential, irrespective of the adopted functional and of the ensuing variation of the band edges.² The defect levels can thus be determined reliably once the host band edges are correctly aligned with respect to the adopted reference. Similarly, the offset of the electrostatic potential at interfaces only depends

on the electron density, which is generally well described in current electronic-structure methods.^{1,8} Therefore the question whether the band edges are correctly positioned acquires prime importance when one resorts to the more accessible hybrid functionals rather than to the GW approximation.

In this work, we systematically investigate the band-edge levels in a large variety of materials as obtained within the most common hybrid functional schemes and the GW approximation to many-body perturbation theory. We take particular care in ensuring a reliable comparison between the two schemes by achieving convergence with respect to the computational parameters and by considering the effect of core electrons. The studied materials (Si, GaAs, AlAs, AlP, GaN, SiC, diamond, AlN, HfO₂, MgO, SiO₂, LiCl, NaF, and LiF) span a large interval of band gaps and show bonding characteristics ranging from purely covalent to highly ionic. In our analysis, we assess the role of dynamic correlation in comparison to that of nonlocal Fock exchange. Furthermore, the common practice of scaling the band gap in hybrid-functional calculations is addressed.

II. METHODS

The present many-body perturbation calculations are performed in the G_0W_0 approximation, in which the eigenfunctions obtained in the semilocal Perdew-Burke-Ernzerhof (PBE) approximation²² are used as starting point and are not further iterated. We use the plasmon-pole approximation (PPM) proposed by Godby and Needs²³ to account for the frequency-dependence of the self-energy. For a subset containing ten of the materials considered, we checked that the full frequency treatment through the analytic continuation of the self-energy along the imaginary axis gives quasiparticle energies differing on average by only 0.05 eV, in accord with other studies.^{8,24} Since it has recently been pointed out that the explicit treatment of core electrons may significantly affect the band gap obtained in the GW scheme,²⁵ we adopt the projector augmented wave (PAW) method, which has been shown to be as accurate as all-electron schemes.²⁶ The PAW data sets are constructed to reproduce the scattering properties up to 20 Ry above the vacuum level. The two outermost shells are included among the valence states for Li, Na, Mg, Al, and Ga. The GW calculations are performed with the ABINIT package.²⁷ The

TABLE I. The numerical parameters of the G_0W_0 calculations: \mathbf{k} -point sampling, ground-state cutoff energy E_{cut} (in Ry), number of (occupied and unoccupied) bands n_{band} used in the dielectric matrix and the Green's function, and cutoff energy $E_{\text{cut}}^{\text{eps}}$ (in Ry) used in the dielectric matrix.

	\mathbf{k} points	E_{cut}	n_{band}	$E_{\text{cut}}^{\text{eps}}$
Si	$12 \times 12 \times 12$	54	500	50
<i>zb</i> -GaAs	$8 \times 8 \times 8$	86	640	30
<i>zb</i> -AlAs	$8 \times 8 \times 8$	90	700	30
<i>zb</i> -AlP	$6 \times 6 \times 6$	78	650	30
3C-SiC	$8 \times 8 \times 8$	56	500	45
4H-SiC	$10 \times 10 \times 6$	56	500	50
<i>zb</i> -GaN	$8 \times 8 \times 8$	86	640	30
<i>wz</i> -GaN	$8 \times 8 \times 6$	86	1000	30
<i>zb</i> -AlN	$6 \times 6 \times 6$	78	650	30
<i>wz</i> -AlN	$8 \times 8 \times 6$	78	700	30
diamond	$8 \times 8 \times 8$	54	260	30
<i>c</i> -HfO ₂	$6 \times 6 \times 6$	68	500	30
<i>m</i> -HfO ₂	$4 \times 4 \times 4$	68	800	30
MgO	$4 \times 4 \times 4$	90	500	30
NaCl	$4 \times 4 \times 4$	68	500	30
SiO ₂	$4 \times 4 \times 4$	66	2000	40
LiCl	$4 \times 4 \times 4$	68	500	40
NaF	$4 \times 4 \times 4$	68	500	40
LiF	$4 \times 4 \times 4$	68	500	40

technical details of the G_0W_0 calculations are summarized in Table I.

In the present study, we employ the Perdew-Burke-Ernzerhof (PBE0)²⁸ and Heyd-Scuseria-Ernzerhof (HSE)²⁹ hybrid functionals. In PBE0, 25% of the PBE exchange is replaced by nonlocal Fock exchange. The HSE hybrid functional also originates from PBE, but nonlocal Fock exchange is only used for describing short-range exchange.²⁹ Core-valence interactions in these hybrid-functional calculations are treated through norm conserving pseudopotentials (NCPs) in which the semicore states are systematically included among the valence states. Such a scheme has been found to yield equivalent results to those achieved with the PAW method,³⁰ in accord with the finding that the explicit treatment of deep core electrons is not critical in Fock exchange calculations.³¹ The band-edge shifts with respect to the PBE calculation are obtained through the alignment of the electrostatic potential. The hybrid-functional calculations are performed with the same \mathbf{k} -point samplings as in the GW scheme, through the use of the QUANTUM ESPRESSO package.³²

III. BAND GAPS

For comparison with previous studies,^{3,5} we present in Fig. 1 and Table II fundamental *band gaps* calculated within our hybrid-functional and G_0W_0 schemes. The calculated band gaps are also compared with corresponding experimental band gaps from various experiments. The G_0W_0 band gaps yield the best agreement with experimental band gaps. Nevertheless, one observes a systematic underestimation, particularly evident for the wide band-gap materials, due to the initial PBE energies used in the one-shot G_0W_0 scheme. For small band-gap semiconductors, HSE also gives a good description,

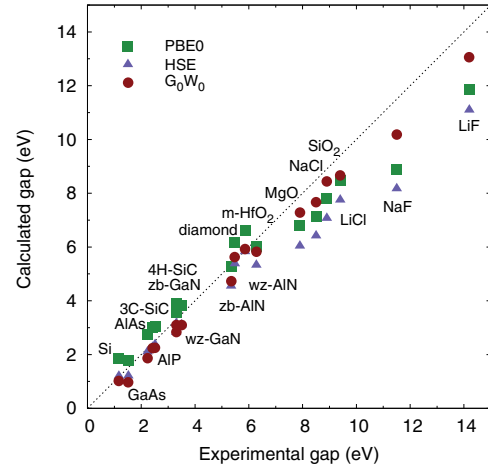


FIG. 1. (Color online) Calculated (PBE0, HSE, G_0W_0) vs experimental band gap for various semiconductors and oxides. The experimental band gaps are referenced in Table II. The PBE lattice parameters are used.

but its performance noticeably deteriorates for wide band-gap materials, with band gaps being underestimated by over 3 eV for LiF and NaF. PBE0 band gaps are larger than HSE ones by about 0.8 eV, following a general rule.³³ The calculated band gaps in Fig. 1 are consistent with previous hybrid functional³ and G_0W_0 (see Ref. 5) results.

IV. BAND-EDGE LEVELS

Next, we focus on the *band-edge levels* as obtained in PBE0, HSE, and G_0W_0 calculations. Figure 2 gives the conduction band minima (CBM) and the valence band maxima (VBM) expressed as band-edge shifts with respect to corresponding levels in the PBE. The figure also shows the VBM shift relative to the band-gap variation, $\Delta E_{\text{VBM}}/\Delta E_{\text{g}}$. The calculated values are also given in Table III. In hybrid-functional calculations, the relative band-edge shift is a characteristic of the functional beyond the value chosen for the mixing parameter α . Indeed, when the states are not significantly modified by Fock exchange, the shift of the band-edge state n is well described by the perturbation expression:

$$\Delta E_n = \langle n | \alpha (\Sigma_x - V_x) | n \rangle, \quad (1)$$

where Σ_x and V_x are the nonlocal Fock and the PBE exchange potential, respectively.⁴⁸ Thus, the CBM and VBM scale linearly with α and the relative shift is independent of α .

It is convenient to focus first on the hybrid-functional results for which the band-edge shifts directly result from the Fock exchange operator. The band-edge shifts calculated in HSE and PBE0 can be discussed on the same footing. Indeed, compared to PBE0, HSE systematically closes the gap in a symmetric way by shifting the CBM and the VBM by 0.3 to 0.4 eV.³³ For the materials studied here, the relative shifts of the VBM range between 50% and 80%. The lowest values correspond to almost symmetric shifts of VBM and CBM and are found for covalent sp materials like Si and diamond. As the ionicity of the material increases, the downward shift of the VBM gradually outweighs the upward shift of the CBM. In particular, we find that different polymorphs generally give

TABLE II. Calculated fundamental band gaps (in eV) of various semiconductors and insulators within the PBE, hybrid-functional (PBE0 and HSE), and G_0W_0 schemes, compared to corresponding experimental band gaps. In particular, the reported experimental values from optical measurements also correspond to fundamental band gaps.

	NCPP			PAW		Expt.
	PBE	PBE0	HSE	PBE	G_0W_0	
Si	0.63	1.84	1.20	0.61	1.01	1.17 ^a
<i>zb</i> -GaAs	0.46	1.78	1.21	0.22	0.97	1.52 ^a
<i>zb</i> -AlAs	1.51	2.73	2.10	1.44	1.87	2.23 ^b
<i>zb</i> -AlP	1.67	3.03	2.37	1.66	2.25	2.51 ^c
3C-SiC	1.40	3.01	2.27	1.35	2.23	2.42 ^d
4H-SiC	2.22	3.88	3.16	2.25	3.10	3.30 ^d
<i>zb</i> -GaN	1.65	3.57	2.83	1.57	2.83	3.30 ^e
<i>wz</i> -GaN	1.91	3.82	3.11	1.74	3.10	3.50 ^f
<i>zb</i> -AlN	3.33	5.26	4.55	3.30	4.73	5.34 ^g
<i>wz</i> -AlN	4.01	6.03	5.33	4.02	5.83	6.28 ^h
diamond	4.22	6.17	5.38	4.13	5.62	5.48 ⁱ
<i>m</i> -HfO ₂	4.19	6.61	5.83	4.09	5.92	5.86 ^j
MgO	4.39	6.80	6.04	4.45	7.28	7.90 ^k
NaCl	5.05	7.15	6.42	5.05	7.67	8.50 ^l
SiO ₂	5.39	7.82	7.07	5.34	8.44	8.90 ^m
LiCl	6.34	8.48	7.75	6.32	8.66	9.40 ⁿ
NaF	6.06	8.90	8.17	6.08	10.19	11.50 ^o
LiF	8.86	11.86	11.10	8.85	13.06	14.20 ^p

^aPhotoluminescence, Ref. 34.

^bPhotoluminescence, Ref. 35.

^cOptical absorption, Ref. 34.

^dPhotoreflectance, Ref. 36.

^ePhotoluminescence, Ref. 37.

^fEllipsometry, Ref. 38.

^gOptical absorption, Ref. 39.

^hPhotoluminescence, Ref. 40.

ⁱPhotoemission, Ref. 41.

^jPhotoreflectance, Ref. 42.

^kPhotoreflectance, Ref. 43.

^lPhotoconductivity on amorphous silica, Ref. 44.

^mPhotoreflectance, Ref. 45.

ⁿElectron energy loss, Ref. 45.

^oThermoreflectance, Ref. 46.

^pThermoreflectance, Ref. 47.

band-edge shifts agreeing within less than 0.05 eV, irrespective of their band-gap difference. For instance, this can be seen for the 3C and 4H forms of SiC, the cubic (*c*) and monoclinic (*m*) forms of HfO₂ and the zinc-blend (*zb*) and wurtzite (*wz*) forms of GaN.

The relation between the calculated band-edge shifts and the underlying physical properties is highly nontrivial because of the complex nature of the Fock exchange operator. However, we remark that the relative band-edge shifts correlate with the character of the band-edge states. A symmetric band-gap opening occurs in covalent materials, when the VBM and CBM are formed by bonding and antibonding combinations of the same atomic *p* orbitals. At variance, the VBM and CBM shifts are uneven in ionic insulators (e.g., the oxides and halides), where the VBM mainly originates from the *p* orbitals of the anions whereas the CBM carries a more predominant weight

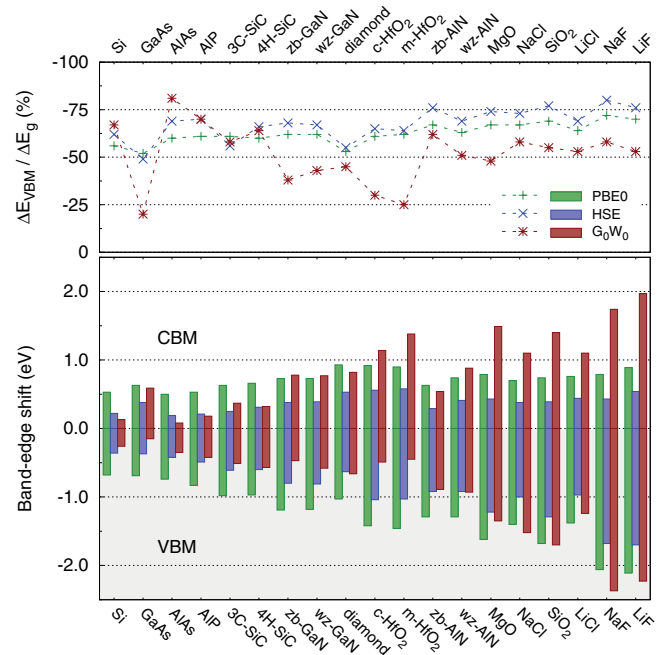


FIG. 2. (Color online) The VBM and CBM levels of semiconductors and insulators as obtained within the hybrid-functional (PBE0 and HSE) and G_0W_0 schemes. The VBM and the CBM are given as shifts, ΔE_{VBM} and ΔE_{CBM} , with respect to the corresponding PBE levels. The top panel gives the relative shift of the VBM with respect to the band gap opening, $\Delta E_{\text{VBM}}/\Delta E_g$.

from either *s* or *d* orbitals. This interpretation accounts for the close shifts calculated in different polymorphs due to the similar characters of their band-edge states. This also explains the relatively large difference (0.1 eV) between the band-edge shifts of the *zb* and *wz* forms of AlN. Indeed, the *s*-character weight of the CBM occurring at the Γ point in the *wz* structure differs by as much as 15% with respect to that of the CBM in the *zb* structure, which instead occurs at the *X* point. When the CBM is considered at the Γ point for both polymorphs, the *s*-character weights practically coincide and so do their band-edge shifts.

Figure 2 also shows the band-edge shifts from G_0W_0 calculations. The *sp* semiconductors (Si, AlAs, AlP, and SiC) show G_0W_0 band-edge shifts agreeing within 0.12 eV with the HSE ones. Larger differences are observed for Ga-containing compounds and for the more ionic materials. The relative VBM shift in G_0W_0 covers a much larger interval (20%–80%) than in the hybrid-functional calculations and the band-gap opening becomes more symmetric for materials with large ionicity. Overall, the band-edge shifts obtained within the hybrid-functional and G_0W_0 schemes neither show a general quantitative correspondence nor reveal a systematic relation.

To analyze the differences between the positions of the band-edge levels obtained with the hybrid-functional and G_0W_0 schemes, we partition the G_0W_0 correction to the band-edge levels, ΔE , into an exchange $\Delta E_x = \langle n | \Sigma_x - V_x | n \rangle$ and a correlation part $\Delta E_c = \langle n | \Sigma_c - V_c | n \rangle$, where $\Sigma_c = iGW - \Sigma_x$ and V_c is the PBE correlation potential. The G_0W_0 correction from the exchange part coincides with the hybrid-functional band-edge shift in Eq. (1) apart from

TABLE III. VBM (ΔE_v) and CBM shifts (ΔE_c) of semiconductors and insulators as calculated within the hybrid-functional (PBE0 and HSE) and the G_0W_0 schemes. The shifts are given with respect to PBE results. The relative VBM shift $\Delta E_v/\Delta E_g$ is also given. Energies are in electron volts.

	PBE0			HSE			G_0W_0		
	ΔE_v	ΔE_c	$\Delta E_v/\Delta E_g$	ΔE_v	ΔE_c	$\Delta E_v/\Delta E_g$	ΔE_v	ΔE_c	$\Delta E_v/\Delta E_g$
Si	-0.68	0.53	-56%	-0.36	0.22	-62%	-0.26	0.13	-67%
<i>zb</i> -GaAs	-0.69	0.63	-52%	-0.37	0.38	-49%	-0.15	0.59	-20%
<i>zb</i> -AlAs	-0.74	0.50	-60%	-0.42	0.19	-69%	-0.35	0.08	-81%
<i>zb</i> -AlP	-0.83	0.53	-61%	-0.49	0.21	-70%	-0.42	0.18	-70%
3C-SiC	-0.98	0.63	-61%	-0.61	0.25	-56%	-0.51	0.37	-58%
4H-SiC	-0.97	0.66	-60%	-0.60	0.31	-66%	-0.57	0.32	-64%
<i>zb</i> -GaN	-1.19	0.73	-62%	-0.80	0.38	-68%	-0.47	0.78	-38%
<i>wz</i> -GaN	-1.18	0.73	-62%	-0.81	0.39	-67%	-0.58	0.77	-43%
<i>zb</i> -AlN	-1.29	0.63	-67%	-0.92	0.29	-76%	-0.89	0.54	-62%
<i>wz</i> -AlN	-1.29	0.74	-63%	-0.92	0.41	-69%	-0.93	0.88	-51%
diamond	-1.03	0.93	-53%	-0.63	0.53	-55%	-0.66	0.82	-45%
<i>c</i> -HfO ₂	-1.42	0.92	-61%	-1.04	0.56	-65%	-0.49	1.14	-30%
<i>m</i> -HfO ₂	-1.46	0.90	-62%	-1.03	0.58	-64%	-0.45	1.38	-25%
MgO	-1.62	0.79	-67%	-1.22	0.43	-74%	-1.35	1.49	-48%
NaCl	-1.40	0.70	-67%	-1.00	0.38	-73%	-1.52	1.10	-58%
SiO ₂	-1.68	0.74	-69%	-1.29	0.39	-77%	-1.70	1.40	-55%
LiCl	-1.38	0.76	-64%	-0.97	0.44	-69%	-1.24	1.10	-53%
NaF	-2.06	0.79	-72%	-1.68	0.43	-80%	-2.37	1.74	-58%
LiF	-2.11	0.89	-70%	-1.70	0.54	-76%	-2.23	1.97	-53%

the scaling factor α . The correlation part is responsible for all the dynamic interactions which are not included in Σ_x . ΔE_c generally compensates the overcorrection achieved by ΔE_x bringing the VBM and CBM back toward midgap. The degree of compensation allows us to draw a connection with hybrid-functional results. When the compensation precisely corresponds to 75%, the band edges calculated within G_0W_0 coincide with those obtained in PBE0, in which only 25% of nonlocal exchange is considered.

Figure 3 shows ΔE_c vs ΔE_x for the VBM and CBM of the considered materials. The degree of compensation is clearly both material and band-edge dependent. For the VBM, the compensating ΔE_c generally lies in a relatively narrow interval

around 80% of ΔE_x . In particular, for the more ionic materials, the compensation is close to 75% and the PBE0 band edges lie close to the ones obtained within G_0W_0 (cf. Fig. 2). The *p-d* coupling in the VBM of HfO₂ results in an exceptionally high degree of compensation ($\sim 90\%$), which is responsible for the noticeable difference between the VBM position in PBE0 and G_0W_0 (cf. Fig. 2). At variance, the ratio $\Delta E_c/\Delta E_x$ for the CBM is much more scattered, ranging from $\sim 95\%$ for the small band-gap semiconductors to less than 50% for some of the most ionic insulators. These results indicate that the CBM in hybrid-functional calculations can generally not well be described with a constant fraction of nonlocal exchange α . For the small band-gap materials, the CBM shift obtained within G_0W_0 is very small as a result of the almost complete cancellation between ΔE_x and ΔE_c (cf. Figs. 2 and 3). In GaAs and GaN, the CBM characterized by anionic *s*-like states is subject to *s-d* coupling, which upsets the compensation leading to a larger band-edge shift. For materials of large ionicity, the CBM shifts are even more pronounced, requiring α values as high as 40%–60% for a proper description in hybrid-functional calculations. Because of this effect, PBE0 and HSE calculations underestimate the CBM shifts obtained within G_0W_0 , and consequently yield higher relative VBM shifts (cf. Fig. 2). These considerations illustrate the limitation of hybrid-functional calculations in which the optimal value of α should not only be material dependent but also band-edge dependent.

It is of interest to address the common practice of scaling the band gap in hybrid-functional calculations. For each material, we thus adapt the fraction of Fock exchange to match the band gap found within G_0W_0 . In Fig. 4, we show the deviations of the hybrid-functional VBM levels from the corresponding G_0W_0 ones. For the *sp* semiconductors (Si, AlAs, AlP, and SiC), the agreement is remarkably good with differences

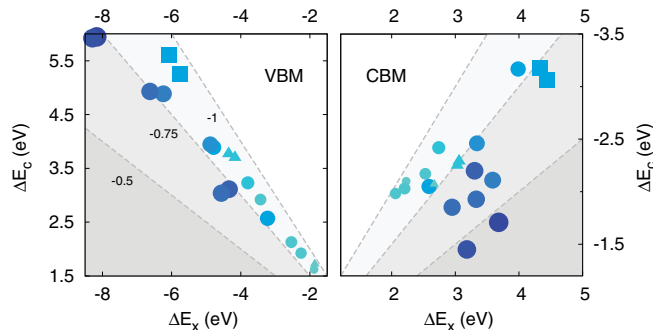


FIG. 3. (Color online) Correlation correction ΔE_c vs exchange correction ΔE_x as obtained within G_0W_0 for the VBM and CBM. The three dividing lines (with slopes of -1 , -0.75 , and -0.5) indicate the degree of compensation between ΔE_x and ΔE_c . The size and the darkness of the symbols scale with the band gap of the material represented. Materials including semicore *d* states are highlighted by squares (HfO₂) and triangles (Ga-based compounds).

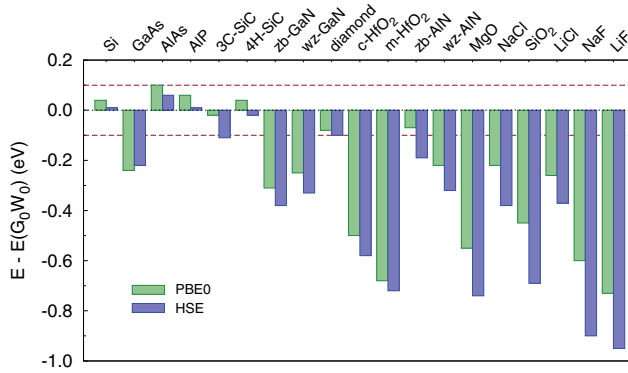


FIG. 4. (Color online) Deviations of the hybrid-functional VBM levels from the corresponding G_0W_0 ones for the materials studied in this work. In the hybrid-functional calculations, the fraction of Fock exchange is adapted to match the corresponding G_0W_0 band gap.

smaller than 0.1 eV. However, the deviations increase for the other materials. For compounds including semicore d states, such as GaAs and GaN, we find differences of ~ 0.25 eV. For the wide band-gap insulators, the band-gap opening within G_0W_0 occurs in a more symmetric fashion than in hybrid-functional schemes, leading to sizable level deviations ranging from 0.5 to 1 eV.

V. CONCLUSIONS

Our results indicate that the band-edge positions obtained with hybrid functionals generally do not agree with reference GW calculations. Nevertheless, we record remarkable agreement for sp -bonded materials with band edges coinciding within 0.1 eV. However, the occurrence of semicore d states or the increase of the ionicity lead to deviations reaching up to 1 eV. Hence, depending on the electronic-structure method used, band alignments might vary significantly, particularly when materials of high ionicity are involved. The comparison with experiment is hindered by the fact that the band-edge shifts are not directly accessible. Further investigations of higher complexity are necessary to assess the overall accuracy of the calculated band-edge shifts through the consideration of defect levels or band offsets.

ACKNOWLEDGMENTS

We acknowledge useful discussions with A. Alkauskas, P. Broqvist, H.-P. Komsa, and G.-M. Rignanese. We used computational resources of CSEA-EPFL, partially supported by the Swiss National Science Foundation (Grant No. 206021-128743).

- ¹A. Alkauskas, P. Broqvist, F. Devynck, and A. Pasquarello, *Phys. Rev. Lett.* **101**, 106802 (2008); P. Broqvist, A. Alkauskas, and A. Pasquarello, *Appl. Phys. Lett.* **92**, 132911 (2008).
- ²A. Alkauskas, P. Broqvist, and A. Pasquarello, *Phys. Rev. Lett.* **101**, 046405 (2008).
- ³A. Alkauskas, P. Broqvist, and A. Pasquarello, *Phys. Status Solidi B* **248**, 775 (2011).
- ⁴M. S. Hybertsen and S. G. Louie, *Phys. Rev. B* **34**, 5390 (1986).
- ⁵M. Shishkin and G. Kresse, *Phys. Rev. B* **75**, 235102 (2007).
- ⁶L. Hedin, *Phys. Rev.* **139**, A796 (1965).
- ⁷S. B. Zhang, M. L. Cohen, S. G. Louie, D. Tománek, and M. S. Hybertsen, *Phys. Rev. B* **41**, 10058 (1990).
- ⁸R. Shaltaf, G.-M. Rignanese, X. Gonze, F. Giustino, and A. Pasquarello, *Phys. Rev. Lett.* **100**, 186401 (2008).
- ⁹M. Grüning, R. Shaltaf, and G.-M. Rignanese, *Phys. Rev. B* **81**, 035330 (2010).
- ¹⁰S. Ismail-Beigi and S. G. Louie, *Phys. Rev. Lett.* **95**, 156401 (2005).
- ¹¹M. Hedström, A. Schindlmayr, G. Schwarz, and M. Scheffler, *Phys. Rev. Lett.* **97**, 226401 (2006).
- ¹²P. Rinke, A. Janotti, M. Scheffler, and C. G. Van de Walle, *Phys. Rev. Lett.* **102**, 026402 (2009).
- ¹³L. Martin-Samos, G. Roma, P. Rinke, and Y. Limoge, *Phys. Rev. Lett.* **104**, 075502 (2010).
- ¹⁴F. Bruneval and G. Roma, *Phys. Rev. B* **83**, 144116 (2011).
- ¹⁵J. M. Knaup, P. Deák, T. Frauenheim, A. Gali, Z. Hajnal, and W. J. Choyke, *Phys. Rev. B* **72**, 115323 (2005).
- ¹⁶K. Xiong, J. Robertson, M. C. Gibson, and S. J. Clark, *Appl. Phys. Lett.* **87**, 183505 (2005).
- ¹⁷P. Broqvist and A. Pasquarello, *Appl. Phys. Lett.* **89**, 262904 (2006).
- ¹⁸A. Wadehra, J. W. Nicklas, and J. W. Wilkins, *Appl. Phys. Lett.* **97**, 092119 (2010).
- ¹⁹P. Mori-Sánchez, A. J. Cohen, and W. Yang, *Phys. Rev. Lett.* **100**, 146401 (2008).
- ²⁰A. Alkauskas and A. Pasquarello, *Phys. Rev. B* **84**, 125206 (2011).
- ²¹H.-P. Komsa and A. Pasquarello, *Phys. Rev. B* **84**, 075207 (2011).
- ²²J. P. Perdew, K. Burke, and M. Ernzerhof, *Phys. Rev. Lett.* **77**, 3865 (1996).
- ²³R. W. Godby and R. J. Needs, *Phys. Rev. Lett.* **62**, 1169 (1989).
- ²⁴M. Stankovski, G. Antonius, D. Waroquiers, A. Miglio, H. Dixit, K. Sankaran, M. Giantomassi, X. Gonze, M. Côté, and G.-M. Rignanese, *Phys. Rev. B* **84**, 241201 (2011).
- ²⁵R. Gómez-Abal, X. Li, M. Scheffler, and C. Ambrosch-Draxl, *Phys. Rev. Lett.* **101**, 106404 (2008).
- ²⁶M. Shishkin and G. Kresse, *Phys. Rev. B* **74**, 035101 (2006).
- ²⁷X. Gonze, B. Amadon, P.-M. Anglade, J.-M. Beuken, F. Bottin, P. Boulanger, F. Bruneval, D. Caliste, R. Caracas, M. Côté, T. Deutsch, L. Genovese, Ph. Ghosez, M. Giantomassi, S. Goedecker, D. R. Hamann, P. Hermet, F. Jollet, G. Jomard, S. Leroux, M. Mancini, S. Mazevet, M. J. T. Oliveira, G. Onida, Y. Pouillon, T. Rangel, G.-M. Rignanese, D. Sangalli, R. Shaltaf, M. Torrent, M. Verstraete, G. Zerah, and J. W. Zwanziger, *Comput. Phys. Commun.* **180**, 2582 (2009).
- ²⁸J. P. Perdew, M. Ernzerhof, and K. Burke, *J. Chem. Phys.* **105**, 9982 (1996).
- ²⁹J. Heyd, G. E. Scuseria, and M. Ernzerhof, *J. Chem. Phys.* **118**, 8207 (2003); **124**, 219906 (2006).
- ³⁰A. Stroppa and G. Kresse, *New J. Phys.* **10**, 063020 (2008).
- ³¹E. Engel, *Phys. Rev. B* **80**, 161205 (2009); A. Makmal, R. Armiento, E. Engel, L. Kronik, and S. Kümmel, *ibid.* **80**, 161204 (2009).

- ³²P. Giannozzi, S. Baroni, N. Bonini, M. Calandra, R. Car, C. Cavazzoni, D. Ceresoli, G. L. Chiarotti, M. Cococcioni, I. Dabo, A. Dal Corso, S. de Gironcoli, S. Fabris, G. Fratesi, R. Gebauer, U. Gerstmann, C. Gougoussis, A. Kokalj, M. Lazzeri, L. Martin-Samos, N. Marzari, F. Mauri, R. Mazzarello, S. Paolini, A. Pasquarello, L. Paulatto, C. Sbraccia, S. Scandolo, G. Sclauzero, A. P. Seitsonen, A. Smogunov, P. Umari, and R. M. Wentzcovitch, *J. Phys.: Condens. Matter* **21**, 395502 (2009).
- ³³H.-P. Komsa, P. Broqvist, and A. Pasquarello, *Phys. Rev. B* **81**, 205118 (2010).
- ³⁴O. Madelung, *Semiconductor-Basic Data*, 2nd ed. (Springer, New York, 1996).
- ³⁵B. Monemar, *Phys. Rev. B* **8**, 5711 (1973).
- ³⁶G. Ramirez-Flores, H. Navarro-Contreras, A. Lastras-Martinez, R. C. Powell, and J. E. Greene, *Phys. Rev. B* **50**, 8433 (1994).
- ³⁷B. Monemar, *Phys. Rev. B* **10**, 676 (1974).
- ³⁸M. P. Thompson, G. W. Auner, T. S. Zheleva, K. A. Jones, S. J. Simko, and J. N. Hilfiker, *J. Appl. Phys.* **89**, 3331 (2001).
- ³⁹P. B. Perry and R. F. Rutz, *Appl. Phys. Lett.* **33**, 319 (1978).
- ⁴⁰P. J. Dean, *Phys. Rev.* **139**, A588 (1965).
- ⁴¹S. Sayan, T. Emge, E. Garfunkel, X. Zhao, L. Wielunski, R. A. Bartynski, D. Vanderbilt, J. S. Suehle, S. Suzer, and M. Banaszak-Holl, *J. Appl. Phys.* **96**, 7485 (2004).
- ⁴²M. W. Williams and E. T. Arakawa, *J. Appl. Phys.* **38**, 5272 (1967).
- ⁴³N. O. Lipari and A. B. Kunz, *Phys. Rev. B* **3**, 491 (1971).
- ⁴⁴T. DiStefano and D. Eastman, *Solid State Commun.* **9**, 2259 (1971).
- ⁴⁵G. Baldini and B. Bosacchi, *Phys. Status Solidi B* **38**, 325 (1970).
- ⁴⁶G. Roy, G. Singh, and T. Gallon, *Surf. Sci.* **152**, 1042 (1985).
- ⁴⁷M. Piacentini, D. W. Lynch, and C. G. Olson, *Phys. Rev. B* **13**, 5530 (1976).
- ⁴⁸In HSE, Σ_x and V_x correspond to the short-range components.